COMMUNICATION

Nanosynthesis

NANO · MICRO
small
www.small-journal.com

Check for updates

A New Type of Capping Agent in Nanoscience: Metal Cations

Jiawei Liu, Shaoyan Wang, Kai Cai, Yefei Li, Zhipan Liu, Lingmei Liu, Yu Han, Hong Wang, Heyou Han,* and Hongyu Chen*

Capping agents are the essential factor in nanoscience and nanotechnology. However, the types of capping agents are greatly limited. Defying conventional beliefs, here is shown that metal cations can also be considered as capping agents for oxide nanoparticles, particularly in maintaining their colloidal stability and controlling their facets. Here the general stabilizing effects of multivalent cations for oxide nanoparticles, and the facet controlling role of Al^{3+} ions in the growth and ripening of Cu_2O octahedra, are demonstrated. This discovery broadens the view of capping agent and opens doors for nanosynthesis, surface treatment, and beyond.

In nanoscience and nanotechnology, capping agents are essential in stabilizing the ultrasmall surfaces of nanocrystals, allowing the synthesis and application of nanomaterials.[1–10] More specifically, they control the surface charge and facets, and maintain the colloidal stability of nanoparticles.[11–15]

Polyvinylpyrrolidone (PVP), a typical surfactant molecule, was initially used as a stabilizer in nanosynthesis, giving only spherical particles.[16,17] As its specific affinity to nanocrystal facets was discovered, PVP served not only as a stabilizing agent but also as a means to control the growth of nanocrystals, introducing a series of new morphologies, such as Ag nanocubes[18] and Ag nanowires.[19] Similarly, Ag nanoplates and Pd nanoplates were successfully synthesized by using citrate[20] and CO[21] as capping agents, respectively. Thus, the facet-controlling ability of capping agents is of great importance

for morphological design of nanoarchitecture, a bottleneck in nanosynthesis. Notwithstanding these progresses, the type and variety of capping agents are still greatly limited, preventing broader exploration. The major role of capping agents in nanosynthesis is to control surface charge and facet growth.[22] For these purposes, all surface-adsorbing species are potential candidates.

Metal ions have been used in nanosynthesis, but rarely as capping agents. For example, Ag^+ ions can facilitate the 1D growth of Au nanorods by forming Au–Ag alloys;[23] Fe^{3+} ions are important to the formation of Pt nanowire as oxidant;[24] Al^{3+} ions are essential for the synthesis of CuSe nanocubes, but is known to only involve in the initial stage.[25] In a pioneer work, metal ions complexed with halide ions ($InCl_3$, $PbBr_2$, $KPbI_3$, etc.) were regarded as a type of "inorganic capping agent" as they could bind to semiconductor nanoparticles (PbS, CdSe, CdS, etc.).[26] The $-InCl_3$ or $-PbI_3$ moieties rendered the nanoparticles with negative changes, by capping the exposed S/Se atoms via coordination bonds.[27] This mode of binding cannot be directly applied to oxides with the harder O as the anion.

Herein, we show that multivalent metal ions (Al^{3+}, Yb^{3+}, In^{3+}, Ca^{2+}, Pb^{2+}) have general affinity for oxide surface, often changing the initially negatively charged surface to positive charges. More specifically, Al^{3+} ions behave like a capping

Dr. J. W. Liu, Dr. K. Cai, Prof. H. Y. Han
State Key Laboratory of Agricultural Microbiology
College of Science
College of Engineering
Huazhong Agricultural University
Wuhan 430070, P. R. China
E-mail: hyhan@mail.hzau.edu.cn

Dr. J. W. Liu, S. Y. Wang, Prof. H. Chen
Division of Chemistry and Biological Chemistry
Nanyang Technological University
Singapore 637371, Singapore

Prof. Y. F. Li, Prof. Z. P. Liu
Collaborative Innovation Center of Chemistry for Energy Material
Shanghai Key Laboratory of Molecular Catalysis and Innovative Materials
Key Laboratory of Computational Physical Science (Ministry of Education)
Department of Chemistry
Fudan University
Shanghai 200433, P. R. China

Dr. L. M. Liu, Prof. Y. Han
Advanced Membranes and Porous Materials Center
Physical Sciences and Engineering Division
King Abdullah University of Science and Technology
Thuwal 23955-6900, Kingdom of Saudi Arabia

Prof. H. Wang, Prof. H. Chen
Institute of Advanced Synthesis
School of Chemistry and Molecular Engineering
Jiangsu National Synergetic Innovation Center for Advanced Materials
Nanjing Tech University
Nanjing 211816, P. R. China
E-mail: iashychen@njtech.edu.cn

ADVANCED
SCIENCE NEWS
www.advancedsciencenews.com

NANO · MICRO
small
www.small-journal.com

agent, in terms of increasing the colloidal stability and control-ling the facet growth of Cu_2O nanoparticles, giving Cu_2O octa-hedra enclosed by (111) facets. The adsorption of Al^{3+} ions on Cu_2O nanoparticles is supported by multiple lines of evidence. Such a discovery opens a new direction for the exploration of capping agent and facet control.

The interaction between metal cations and oxides was dis-covered in the synthesis of Cu_2O nanoparticles in an attempt to modify the method.[28] The reduction of $Cu(NO_3)_2$ by $NaBH_4$ gave visible precipitate in about 90 s (**Figure 1**a), whereas in the presence of $Al(NO_3)_3$, this reaction gave clear solution without any precipitate (Figure 1b). As the net concentrations of NO_3^- anions are similar in the two reactions, Al^{3+} appears to be the key factor. As the degree of hydrolysis of Al^{3+} ions was

only about 1.4%, the possible function of hydrolyzed hydrox-ides could also be ignored (Figure S1, Supporting Information). The degree of Cu_2O aggregation under different Al^{3+} concentra-tion was characterized by dynamic light scattering (DLS). The range of nanoparticle distribution and average nanoparticle size were both reduced with the increase of Al^{3+} concentration (Figure 1c), further indicating that Al^{3+} ions are able to prevent the aggregation of Cu_2O nanoparticles.

Thus, we hypothesized that Al^{3+} ions can adsorb on the sur-face of Cu_2O nanoparticles, enhancing their surface charge and colloidal stability. To investigate the issue of Al^{3+} adsorp-tion, the zeta potential of the Cu_2O nanoparticles synthesized under different concentration of Al^{3+} ions was first studied. In the presence of 0, 12.5, 25, 37.5, 50, and 62.5×10^{-6} M $Al(NO_3)_3$,
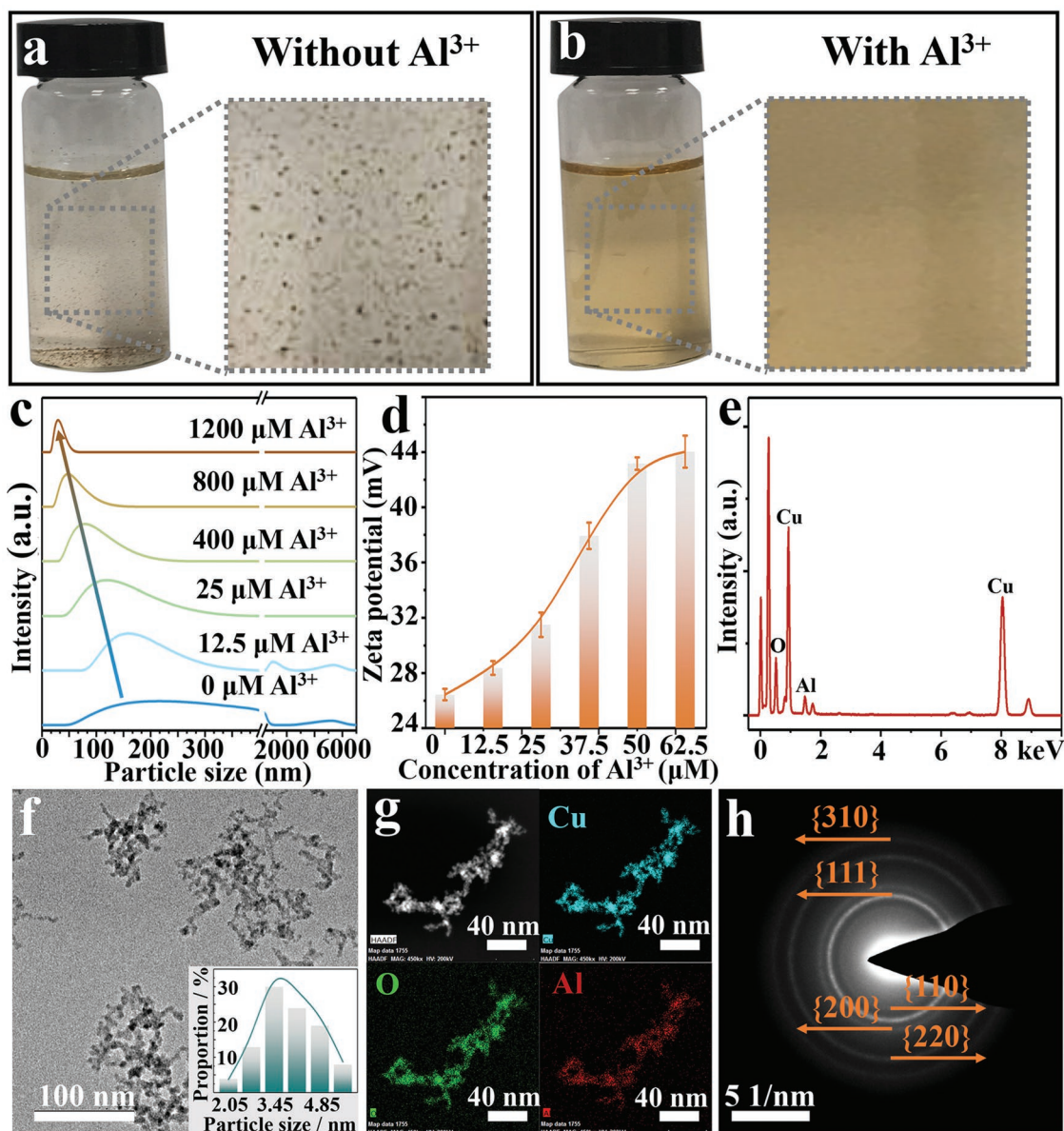

Figure 1. The photographs of reaction solution for synthesizing Cu_2O nanoparticles: a) in the absence of Al^{3+}, b) in the presence of Al^{3+}. c) The particle size and d) zeta potential of Cu_2O nanoparticles made with different $[Al^{3+}]$. e) The EDX, f) TEM, g) HAADF element mapping, and h) SAED of Cu_2O nanoparticles made with 50×10^{-6} M Al^{3+}. The inset bar graph in Figure 1f was the particle size distribution of corresponding Cu_2O nanoparticles.

ADVANCED
SCIENCE NEWS
www.advancedsciencenews.com

NANO · MICRO
small
www.small-journal.com

aqueous $Cu(NO_3)_2$ solution was reduced by $NaBH_4$. After 5 min, the zeta potential of the reaction solution was directly measured. As shown in Figure 1d, with increasing concentration of Al^{3+} ions, the zeta potential of Cu_2O nanoparticles increased from +26.4 to +44 mV. In a control experiment, the aqueous $Al(NO_3)_3$ solution by itself with increasing concentration did not cause obvious change in zeta potential (Figure S2, Supporting Information), ruling out the possible interference of Al^{3+} in the solution. Hence, this contrast supports the adsorption of Al^{3+} ions on Cu_2O surface.

After being washed twice and redispersed in ethanol, the Al^{3+} adsorbed Cu_2O nanoparticles were able to remain unchanged for a long time. The transmission electron microscopy (TEM) image showed that there were no other impurities in product, only nanoparticles of 4.0 nm in diameter (Figure 1f and Figure S3, Supporting Information). The precipitate and its supernatant were characterized by inductively coupled plasma mass spectrometry (ICP-MS), showing that the majority of the Al^{3+} ions were adsorbed on the precipitates, which was further proved by energy dispersive X-ray spectroscopy (EDX) and high-angle annular dark-field scanning transmission electron microscopy (HAADF-STEM) elemental mapping. The Al to Cu atom ratio was about 1:6 in both EDX (Figure 1g) and ICP-MS (Table S1, Supporting Information). In a simplified model, a Cu_2O nanosphere of 4 nm in diameter covered with a monolayer of Al^{3+} gives a theoretical atom ratio of 1:4.4, which is roughly consistent with the above ratio. The homogeneous distribution of Al and Cu elements was shown in Figure 1g, excluding the presence of individual Al compounds in the solution.

To verify the assignment of Cu_2O in those nanoparticles, their ultraviolet-visible (UV-vis) spectra, X-ray diffraction (XRD), and selected area electron diffraction (SAED) were measured. The nanoparticles had a strong and broad UV–vis adsorption from 200–500 nm (Figure S4, Supporting Information), which agreed with the characteristic adsorptions of Cu_2O nanoparticles.[29]

The SAED of multiple nanoparticles gave ring patterns consistent with Cu_2O scattering angles (Figure 1e). The purity and composition of the product was proved by XRD (Figure S5, Supporting Information). There were no unassigned peaks except several peaks that are characteristic of Cu_2O, ruling out the presence of crystalline impurities, significant doping, or alloying. In high resolution transmission electron microscope (HRTEM) image, the characteristic Cu_2O lattice on the edge of nanoparticles shows that there is no amorphous layer on the product surface (Figure S6, Supporting Information).

Besides, other cations (such as Fe^{3+}, In^{3+}, Ni^{2+}, and Ca^{2+}) were also able to prevent the aggregation of Cu_2O nanoparticles in similar synthesis, inspiring us to study the general adsorption effect of cations to oxide nanocrystals. Citric acid-stabilized Fe_3O_4 nanoparticles were synthesized through a capping agent exchange process from oleic acid stabilized Fe_3O_4 nanoparticles.[30] PVP-modified MnO and ZnO nanoparticles were prepared by thermal decomposition of aqueous $Mn(CH_3COO)_2$ and $Zn(NO_3)_2$ at 95 °C.[31] Silica nanoparticles were prepared by first hydrolyzing tetraethyl orthosilicate (TEOS) in 75% ethanol in aqueous solution, and then washed with acid solution.[32] Capping agent-free TiO_2 nanorods were synthesized by a calcination process under 825 °C.[33] The morphology of these nanoparticles was characterized by TEM (**Figure 2**a).

To study the interaction between Al^{3+} ions and oxide nanoparticles, varying amount of $Al(NO_3)_3$ (0, 25, 50, 75, 100, and 125×10^{-6} M) was mixed with citric acid-stabilized Fe_3O_4 nanoparticles for 1 h, and zeta potential of the resulting solution was measured. The surface charge of Fe_3O_4 nanoparticles increased from −26.9 to +17.5 mV, with a similar trend as those of Cu_2O nanoparticles (Figure 2b). Repeating experiments gave three similar traces of surface charge (Figure S7, Supporting Information), supporting the reliability of the surface treatment. Interestingly, other oxide nanoparticles such as PVP-modified MnO and ZnO, acid-treated silica, and clean surface
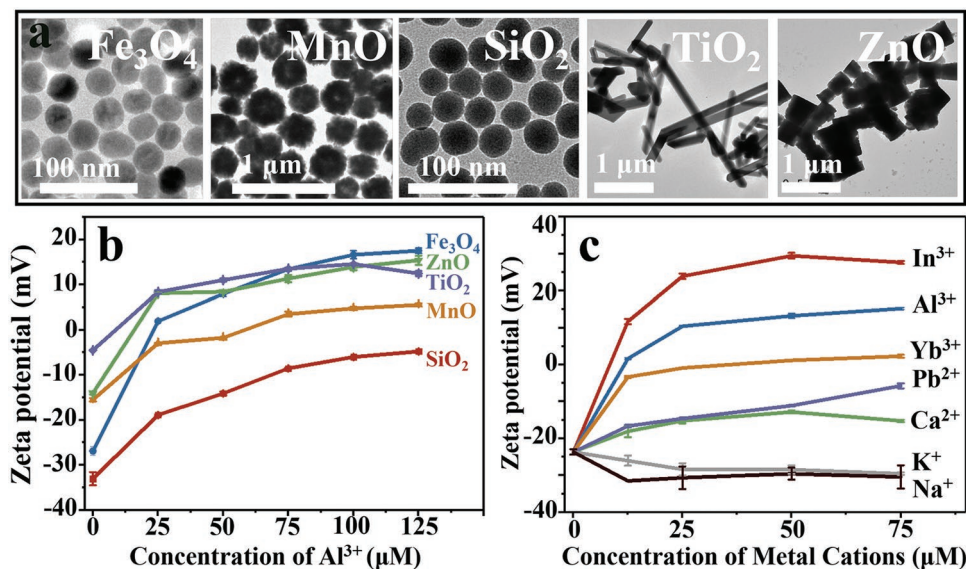

Figure 2. a) TEM images of different oxide nanoparticles: citric acid-stabilized Fe_3O_4 nanobeads, PVP-modified MnO (ZnO), silica nanospheres, and TiO_2 nanorods. b) Zeta potential of different oxide nanoparticles under the influence of increasing $[Al^{3+}]$. c) Zeta potential of Fe_3O_4 nanoparticles under the influence of different cations: In^{3+}, Al^{3+}, Yb^{3+}, Pb^{2+}, Ca^{2+}, K^+, and Na^+.

ADVANCED
SCIENCE NEWS
www.advancedsciencenews.com
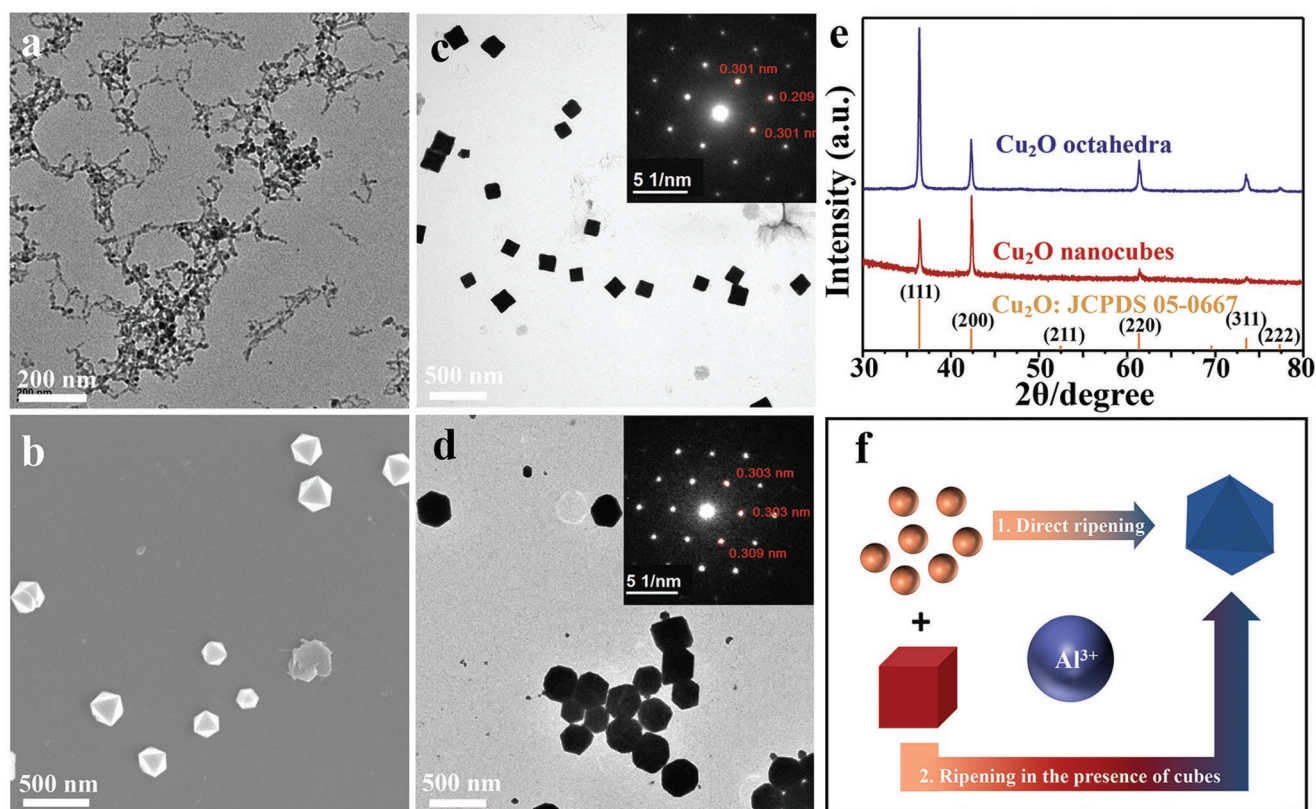
NANO · MICRO
small
www.small-journal.com

Figure 3. a) TEM image of primary Cu_2O nanoparticles; and b) SEM image of Cu_2O octahedra obtained by direct ripening process. TEM image and SAED of c) Cu_2O nanocube seeds and d) the resulting octahedra obtained in a seeded ripening process. e) XRD pattern of Cu_2O nanocubes and octahedra. f) Schematics showing two cases of facet transformation controlled by Al^{3+} ions.

TiO_2 nanoparticles all behaved like the Fe_3O_4 nanoparticles, with increasing surface charge at higher Al^{3+} concentrations (Figure 2b). Therefore, Al^{3+} ion does indeed have strong affinity to oxides, independent of their surface capping agents.

Then, the adsorption of other metal cations (Yb^{3+}, In^{3+}, Ca^{2+}, Pb^{2+}, K^+, and Na^+) to oxide was studied by the same method (Figure 2c). Citric acid-stabilized Fe_3O_4 nanoparticles were selected as a model system for the following reasons: 1) the range of surface charge variation in the Al^{3+} case is very large, facilitating the observation of trends; 2) its surface capping agent after the capping agent exchange from oil to water phase can be easily assigned, reducing the ambiguity caused by uncertain capping agents.

As shown in Figure 2c, trivalent ions (Al^{3+}, Yb^{3+}, and In^{3+}) caused an obvious increase in zeta potential, suggesting their strong affinity to oxide. The interaction between divalent ions (Ca^{2+} and Pb^{2+}) and Fe_3O_4 nanoparticles was less significant according to the moderate increase of zeta potential. Monovalent ions (K^+ and Na^+) barely changed the surface charge of Fe_3O_4 nanoparticles, and the slight decrease of zeta potential may be caused by the shielding effect. Therefore, cations are able to adsorb to oxide surface, especially multivalent cations. The adsorption of Al^{3+} ions to Cu_2O nanocrystals was a general effect caused by the interaction between cations and oxides.

Besides maintaining the colloidal stability of Cu_2O nanoparticles, Al^{3+} ions are also able to control their facet. In a typical synthesis, 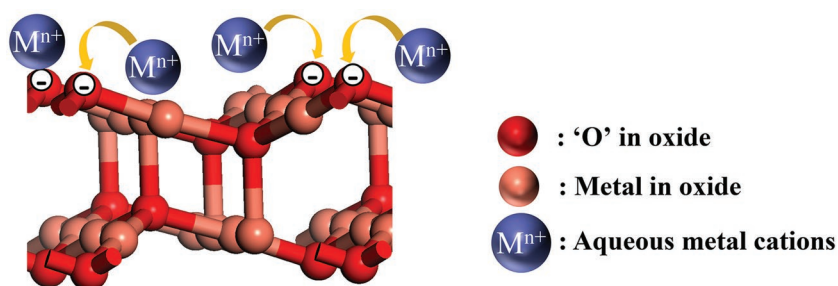aqueous $Cu(NO_3)_2$ was reduced by $NaBH_4$ in the presence of $Al(NO_3)_3$ ($Cu^{2+}/Al^{3+} = 6.25$). TEM images showed that the resulting nanoparticles were about 4 nm in diameter (hereafter referred to as the primary nanoparticles, **Figure 3**a). Then, the primary nanoparticles were isolated by centrifugation, redispersed in water (1/12 of the original volume, or V/12), and incubated for 12 h without shaking, giving well-dispersed Cu_2O octahedra of 170 nm in diameter enclosed by (111) facets (Figure 3b and Figure S8, Supporting Information). Normally, in a Cu_2O nanocrystal with clean surface, (100) facets are more stable than (111) facets, leading to a cube-like structure.[34] Therefore, the octahedral structure can be attributed to the presence of Al^{3+}, altering the surface energy of different facets in the Cu_2O nanocrystals.

The facet controlling ability of Al^{3+} ions was further supported by a ripening process transforming preexisting Cu_2O cubes to octahedra. First, $Cu(NO_3)_2$ was reduced by N_2H_4 to form nanocubes[35] of 140 nm in diameter by a modified method, and the lattice structure of Cu_2O was proven by SAED pattern (Figure 3c). Using these nanocubes as seeds, the primary Cu_2O nanoparticles and $Al(NO_3)_3$ were added in sequence. After stirring for 12 h, the cubes disappeared to give mostly well-dispersed octahedra of 280 nm in diameter (Figure 3d and Figure S9, Supporting Information). The SAED pattern verified that those octahedra were also Cu_2O (Figure 3d). As known in the literature[34,36] and shown in the X-ray diffraction (XRD) results, the (100) peak is stronger than the (111) peak in the samples of Cu_2O nanocube, whereas the

reverse is true for the samples of Cu_2O octahedra (Figure 3e). As described above, Al^{3+} ions facilitated the direct synthesis of Cu_2O octahedra. In comparison, during ripening process, small nanoparticles were dissolved and redeposited onto larger ones. Thus, the primary Cu_2O nanoparticles were dissolved and the Cu_2O nanocube seeds grew larger. As Al^{3+} ions made the (111) facets more stable, the Cu_2O nanocubes gradually became octahedra.

There are two possible mechanisms of Al^{3+} facet control: 1) the H^+ released by Al^{3+} hydrolysis may control the facets of Cu_2O nanocrystals; or 2) Al^{3+} ions may directly adsorb to the surface of Cu_2O nanocrystals exerting their effect. To investigate the pH effect of Al^{3+} hydrolysis, corresponding concentrations of HNO_3 were used to replace the Al^{3+} ions in the synthesis, either during the first step reaction or added to the isolated precipitate (Figure S10, Supporting Information). Only aggregated primary nanoparticles were obtained with no sign of octahedra, ruling out pH as the key factor. Therefore, the surface energy reversal of (111) and (100) facets should be attributed to the adsorption of Al^{3+} ions to Cu_2O nanocrystals.

As showed in **Scheme 1**, metal cations with positive charge could adsorb to the oxygen atoms with partial negative charge on the oxide surface. Density functional theory (DFT) was applied to study the relative stability of (111) and (100) facets of Cu_2O nanocrystals before and after the adsorption of Al^{3+} ions, by calculating the surface energy via using the spin-polarized density functional theory calculation method with the SIESTA code (**Figure 4**).[37] The solvation of surfaces was considered implicitly using a periodic continuum solvation model with a smooth dielectric function. After the adsorption of Al^{3+} ions, the surface energy of (100) and (111) facets decreased from 0.5 and 0.7 $J m^{-2}$ to 0.08 and -0.12 $J m^{-2}$, respectively, indicating that Al^{3+} ions can increase the colloidal stability of Cu_2O nanocrystals. Besides, in the absence of Al^{3+} ions, the (100) facet (0.5 $J m^{-2}$) was intrinsically more stable than the (111) facet (0.7 $J m^{-2}$), because of only "O" termination for the (100) facet, while both "Cu", and "O" atoms terminated on the (111) facet.[34,38] However, the reverse of their stability occurred after the adsorption of Al^{3+}. The (111) facet (-0.12 $J m^{-2}$) became more stable than (100) facet (0.08 $J m^{-2}$), supporting the stabilizing effects of Al^{3+} ions theoretically.

In conclusion, we found that Al^{3+} ions could stabilize Cu_2O nanoparticles and induce (111) facets, similar to the roles of capping agents. The affinity of multivalent metal cations to oxide surface suggests that this could be a general effect. This perspective may inspire new synthetic designs and controlling methods in nanosynthesis, surface treatment, and beyond.
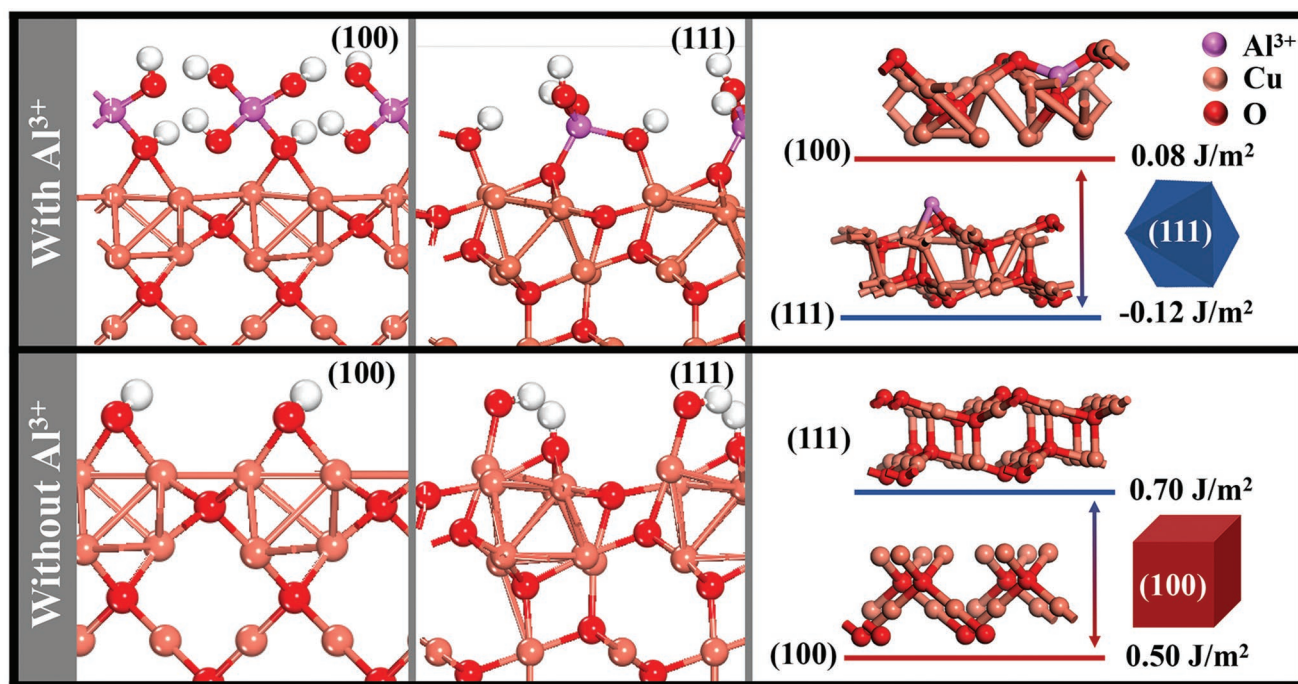

Scheme 1. The absorption of metal cations on oxide surface.

Figure 4. The surface energy of (100) and (111) facets in Cu_2O nanocrystals before and after the adsorption of Al^{3+} ions.

ADVANCED
SCIENCE NEWS
www.advancedsciencenews.com

NANO · MICRO
small
www.small-journal.com

Experimental Section

General: All chemical reagents were used without further purification. Copper nitrate trihydrate [$Cu(NO_3)_2 \cdot 3H_2O$, 99%], aluminum nitrate nonahydrate [$Al(NO_3)_3 \cdot 9H_2O$, 99%], indium nitrate hydrate [$In(NO_3)_3 \cdot xH_2O$, 99%], ytterbium nitrate pentahydrate [$Yb(NO_3)_3 \cdot 5H_2O$, 99%], lead nitrate [$Pb(NO_3)_2$, 99%], calcium nitrate [$Ca(NO_3)_2$, 99%], potassium nitrate (KNO_3, 99%), manganous acetate [$Mn(CH_3COO)_2$, 99%], tetraethoxysilane (TEOS), sodium chloride ($NaCl$, 99%), disodium hydrogen phosphate dodecahydrate ($Na_2HPO_4 \cdot 12H_2O$, 99%), *N*, *N*-Dimethylformamide (DMF), 1,2-dichlorobenzene (DCB, 99%), polyvinyl pyrrolidone (PVP, 40000), titanium oxide nanoparticles (TiO_2 NPs, P25), and hexamethylenetetramine (HMTA) were supplied by Sigma-Aldrich. Sodium nitrate ($NaNO_3$, 99%) was purchased from Alfar Aesar. Ammonium hydroxide ($NH_3 \cdot H_2O$, 25%) was purchased from Sinopharm Chemical Reagent Co., Ltd. Sodium borohydride ($NaBH_4$, 98%) and zinc nitrate hexahydrate [$Zn(NO_3)_2 \cdot 6H_2O$, 99%] were purchased from Strem Chemicals, Inc. Oleic acid-stabilized iron oxide nanoparticles (Fe_3O_4 NPs, $d = 40$ nm) were purchased from Ocean NanoTech. Ethanol (CH_3CH_2OH, 99%) was purchased from Merck. Deionized water (DI water, resistance > 18.2 MΩ cm^{-1}) was used for all experiments.

Synthesis of Cu_2O Nanoparticles: In a typical synthesis, different amount of $Al(NO_3)_3$ (0 and 0.4 µmol) were separately mixed with 2.5 µmol of $Cu(NO_3)_2$ solution in 7.4 mL of H_2O under continuous stirring at 0 °C for 10 min, followed by rapidly injecting 250 µL of fresh-made $NaBH_4$ aqueous solution (1 mg mL^{-1}) and stirring for another 5 min. The yellow products were collected by centrifugation (12 000 rpm, 5 min), washed twice by ethanol, and redispersed into 600 µL of ethanol for preventing further ripening.

Characterization of the Composition of Cu_2O Nanoparticles by ICP-MS: First, 300 uL of above mentioned Cu_2O nanoparticles were separated by centrifugation (12 000 rpm, 5 min) and the supernatant was removed. Then, 0.4 mL of aqua regia was added to dissolve the precipitate and the solution was diluted into 10 mL by deionized water to make ICP-MS test. To exclude the false positive caused by residual supernatant in precipitate, 50 uL of supernatant was also treated by aqua regia and diluted into 10 mL for ICP-MS test.

Characterization of the Particle Size by DLS: In a typical synthesis, different amount of $Al(NO_3)_3$ (0, 0.1, 0.2, 3.2, 6.4, 9.6 µmol) were separately mixed with 2.5 µmol of $Cu(NO_3)_2$ solution in 7.4 mL of H_2O under continuous stirring at 0 °C for 10 min. This was followed by rapidly injecting 250 µL of fresh-made $NaBH_4$ aqueous solution (1 mg mL^{-1}) and stirring for another 5 min. 1 mL of reaction solution was directly taken into a sample cell to measure the particle size using DLS.

Characterization of the Zeta Potential by DLS: In a typical synthesis, different amount of $Al(NO_3)_3$ (0, 0.1, 0.2, 0.3, 0.4, 0.5 µmol) was separately mixed with 2.5 µmol of $Cu(NO_3)_2$ solution in 7.4 mL of H_2O under continuous stirring at 0 °C for 10 min, followed by rapidly injecting 250 µL of fresh-made $NaBH_4$ aqueous solution (1 mg mL^{-1}) and stirring for another 5 min. 1 mL of reaction solution was directly taken into a sample cell to measure the zeta potential using DLS.

Synthesis of Cu_2O Nanoparticles under Other Cations: In a typical synthesis, 0.4 µmol of $FeCl_3$ ($InCl_3$, $Ni(NO_3)_2$, or $CaCl_2$) was mixed with 2.5 µmol of $Cu(NO_3)_2$ solution in 7.4 mL of H_2O under continuous stirring at 0 °C for 10 min, followed by rapidly injecting 250 µL of fresh-made $NaBH_4$ aqueous solution (1 mg mL^{-1}) and stirring for another 5 min. The yellow products were collected by centrifugation (12 000 rpm, 5 min) and washed three times with deionized water, respectively.

Synthesis of the PVP-Modified MnO (or ZnO) Nanoparticles: 40 µmol of $Mn(CH_3COO)_2$ (or $Zn(NO_3)_2$) was mixed with 1.1 of mmol PVP in 10 mL of H_2O, followed by adding 40 µmol of HMTA and stirring at 95 °C for 3 h. The products were collected by centrifugation (14 000 rpm, 5 min) and washed three times with deionized water, respectively.

Synthesis of the Silica Nanospheres: A modified Stöber method was applied to synthesize the silica nanospheres. 250 µL of $NH_3 \cdot H_2O$ (w/w = 25%) was added into 10 mL of ethanol aqueous solution (75%), followed by the addition of 300 µL of TEOS. After stirring for 15 h, the product was collected by centrifugation (14 000 rpm, 2 min), and washed by HNO_3 (0.1 M) for three times.

Synthesis of the Citric Acid-Stabilized Fe_3O_4 Nanobeads: In a typical synthesis, 10 mg of citric acid was added into 2 mL of DMF, followed by the addition of 2 mL of DCB and 625 µg of oleic acid-stabilized Fe_3O_4, and mixed by vortex. After standing at 100 °C for 24 h, the products were collected by magnet and washed three times with deionized water.

Synthesis of the TiO_2 Nanorods: In a typical synthesis, 200 mg of P25 TiO_2 NPs, 200 mg of $NaCl$, and 200 mg of Na_2HPO_4 were mixed in a crucible. This was followed by heating in a furnace under 825 °C for 8 h. After cooling down to room temperature, the products were washed with boiled water for three times and collected by centrifugation (12 000 rpm, 5 min).

Characterization of the Zeta Potential of Oxides: In a typical synthesis, different amount of $Al(NO_3)_3$ (0, 25, 50, 75, 100, 125 nmol) were separately mixed with 300 µg of citric acid-stabilized Fe_3O_4 nanobeads in 1 mL of deionized water. After standing for 60 min, the solution was directly taken into a sample cell to measure the zeta potential using DLS. The zeta potential of other oxides such as PVP-modified MnO (or ZnO), silica nanospheres, and TiO_2 nanorods were measured by replacing citric acid-stabilized Fe_3O_4 nanobeads into above oxides. The zeta potential of citric acid-stabilized Fe_3O_4 nanobeads under other kind of cations were also measured by replacing Al^{3+} ions into In^{3+}, Yb^{3+}, Pb^{2+}, Ca^{2+}, K^+, and Na^+ ions.

Synthesis of the Cu_2O Octahedra: In a typical synthesis, 0.4 µmol of $Al(NO_3)_3$ was mixed with 2.5 µmol of $Cu(NO_3)_2$ solution in 7.4 mL of H_2O under continuous stirring at 0 °C for 10 min. Followed by rapidly injecting 250 µL of fresh-made $NaBH_4$ aqueous solution (1 mg mL^{-1}) and stirring for another 5 min. The yellow products were collected by centrifugation (12 000 rpm, 5 min) and redispersed into 600 µL of deionized water. After standing for 12 h, the products were collected by centrifugation (2000 rpm, 2 min), washed once by 200 µL of deionized water, and redispersed into 200 µL of deionized water for storing.

Synthesis of the Cu_2O Nanocubes: In a typical synthesis, 2.5 µmol of $Cu(NO_3)_2$ solution in 7.4 mL of H_2O under continuous stirring at 25 °C for 10 min, followed by adding 0.01 µmol of N_2H_4 aqueous solution drop by drop and stirring for 5 min. The yellow products were collected by centrifugation (12 000 rpm, 5 min) and redispersed into 600 µL of deionized water.

Ripening in the Presence of Nanocubes: In a typical synthesis, Cu_2O nanoparticles were prepared by mixing 2.5 µmol of $Cu(NO_3)_2$ solution in 7.4 mL of H_2O under continuous stirring at 0 °C for 10 min, followed by rapidly injecting 250 µL of fresh-made $NaBH_4$ aqueous solution (1 mg mL^{-1}) and stirring for another 90 s. The yellow products were collected by centrifugation (12 000 rpm, 5 min) and redispersed into 500 µL of deionized water.

Then, 100 µL of as-prepared Cu_2O nanoparticles were mixed with 300 µL of as-prepared Cu_2O nanocubes. This was followed by adding 5 µL of $Al(NO_3)_3$ aqueous solution (10$\times$ 10^{-6} M) and standing for 12 h. The products were collected by centrifugation (2000 rpm, 2 min), washed once by 200 µL deionized water, and redispersed into 200 µL deionized water for storage.

DFT Calculation: All DFT calculations for geometry relaxation and surface energy were carried out using numerical atomic orbital basis sets and Troullier–Martins norm-conserving pseudopotentials as implemented in SIESTA package.[34] The geometry optimization was based on the exchange-correlation functional GGA-PBE.[36] The geometry convergence criterion was set as 0.08 eV Å^{-1} for the maximal component of force. The k-point mesh utilized was up to (8 × 4 × 1) in the Monkhorst–Pack scheme. The surface energies (γ is calculated by following Equation (1)

$$\gamma = \left(E_{Al(OH)_3/Cu_2O} - E_{Al(OH)_3} - E_{Cu_2O} \right)/A \tag{1}$$

where $E_{Al(OH)_3/Cu_2O}$, $E_{Al(OH)_3}$, and E_{Cu_2O} are total energies for Al^{3+} adsorbed Cu_2O surface, $Al(OH)_3$ molecule, and bulk Cu_2O, respectively. A is area of Cu_2O surface.

Supporting Information

Supporting Information is available from the Wiley Online Library or from the author.

Conflict of Interest

The authors declare no conflict of interest.

Keywords

[1] Z. Niu, Y. Li, *Chem. Mater.* **2014**, *26*, 72.
[2] C.-Y. Chiu, Y. Li, L. Ruan, X. Ye, C. B. Murray, Y. Huang, *Nat. Chem.* **2011**, *3*, 393.
[3] Q. Guo, S. Mo, P. Liu, W. Zheng, R. Qin, C. Xu, Y. Wu, B. Wu, N. Zheng, *Sci. China: Chem.* **2017**, *60*, 1444.
[4] F. Saleem, Z. Zhang, B. Xu, X. Xu, P. He, X. Wang, *J. Am. Chem. Soc.* **2013**, *135*, 18304.
[5] Y. Feng, J. He, H. Wang, Y. Y. Tay, H. Sun, L. Zhu, H. Chen, *J. Am. Chem. Soc.* **2012**, *134*, 2004.
[6] Y. Feng, S. Xing, J. Xu, H. Wang, J. W. Lim, H. Chen, *Dalton Trans.* **2010**, *39*, 349.
[7] Y. Feng, Y. Wang, J. He, X. Song, Y. Y. Tay, H. H. Hng, X. Y. Ling, H. Chen, *J. Am. Chem. Soc.* **2015**, *137*, 7624.
[8] K. Cai, Z. Lv, K. Chen, L. Huang, J. Wang, F. Shao, Y. Wang, H. Han, *Chem. Commun.* **2013**, *49*, 6024.
[9] K. Cai, J. Liu, H. Zhang, Z. Huang, Z. Lu, M. F. Foda, T. Li, H. Han, *Chem. - Eur. J.* **2015**, *21*, 7556.
[10] J. He, Y. Wang, Y. Feng, X. Qi, Z. Zeng, Q. Liu, W. S. Teo, C. L. Gan, H. Zhang, H. Chen, *ACS Nano* **2013**, *7*, 2733.
[11] Q. Li, S. Ji, M. Li, X. Duan, *Sci. China Mater.* **2018**, *61*, 1339.
[12] T. Ling, J. J. Wang, H. Zhang, S. T. Song, Y. Z. Zhou, J. Zhao, X. W. Du, *Adv. Mater.* **2015**, *27*, 5396.
[13] Y. Yin, A. P. Alivisatos, *Nature* **2005**, *437*, 664.
[14] K. Cai, W. Zhang, J. Zhang, H. Li, H. Han, T. Zhai, *ACS Appl. Mater. Interfaces* **2018**, *10*, 36703.
[15] H. Wang, X. Song, C. Liu, J. He, W. H. Chong, H. Chen, *ACS Nano* **2014**, *8*, 8063.
[16] H. H. Huang, X. P. Ni, G. L. Loy, C. H. Chew, K. L. Tan, F. C. Loh, J. F. Deng, G. Q. Xu, *Langmuir* **1996**, *12*, 909.
[17] H. Hirai, *J. Macromol. Sci. A* **1979**, *13*, 633.
[18] Y. G. Sun, Y. N. Xia, *Science* **2002**, *298*, 2176.
[19] Y. Sun, Y. Xia, *Adv. Mater.* **2002**, *14*, 833.
[20] J. E. Millstone, S. J. Hurst, G. S. Metraux, J. I. Cutler, C. A. Mirkin, *Small* **2009**, *5*, 646.
[21] X. Q. Huang, S. H. Tang, X. L. Mu, Y. Dai, G. X. Chen, Z. Y. Zhou, F. X. Ruan, Z. L. Yang, N. F. Zheng, *Nat. Nanotechnol.* **2011**, *6*, 28.
[22] Y. Wang, J. He, C. Liu, W. H. Chong, H. Chen, *Angew. Chem., Int. Ed.* **2015**, *54*, 2022.
[23] B. Nikoobakht, M. A. El-Sayed, *Chem. Mater.* **2003**, *15*, 1957.
[24] J. Y. Chen, T. Herricks, Y. N. Xia, *Angew. Chem., Int. Ed.* **2005**, *44*, 2589.
[25] W. Li, R. Zamani, M. Ibáñez, D. Cadavid, A. Shavel, J. R. Morante, J. Arbiol, A. Cabot, *J. Am. Chem. Soc.* **2013**, *135*, 4664.
[26] D. N. Dirin, S. Dreyfuss, M. I. Bodnarchuk, G. Nedelcu, P. Papagiorgis, G. Itskos, M. V. Kovalenko, *J. Am. Chem. Soc.* **2014**, *136*, 6550.
[27] J. Owen, *Science* **2015**, *347*, 615.
[28] J. Zhang, J. Liu, Q. Peng, X. Wang, Y. Li, *Chem. Mater.* **2006**, *18*, 867.
[29] S. Deki, K. Akamatsu, T. Yano, M. Mizuhata, A. Kajinami, *J. Mater. Chem.* **1998**, *8*, 1865.
[30] W. H. Chong, L. K. Chin, R. L. S. Tan, H. Wang, A. Q. Liu, H. Chen, *Angew. Chem., Int. Ed.* **2013**, *52*, 8570.
[31] H. Sun, J. He, J. Wang, S.-Y. Zhang, C. Liu, T. Sritharan, S. Mhaisalkar, M.-Y. Han, D. Wang, H. Chen, *J. Am. Chem. Soc.* **2013**, *135*, 9099.
[32] W. Stöber, A. Fink, E. Bohn, *J. Colloid Interface Sci.* **1968**, *26*, 62.
[33] B. Liu, H. M. Chen, C. Liu, S. C. Andrews, C. Hahn, P. Yang, *J. Am. Chem. Soc.* **2013**, *135*, 9995.
[34] W. Z. Wang, W. Gang, X. S. Wang, Y. Zhan, Y. Liu, C. L. Zheng, *Adv. Mater.* **2002**, *14*, 67.
[35] D.-F. Zhang, H. Zhang, L. Guo, K. Zheng, X.-D. Han, Z. Zhang, *J. Mater. Chem.* **2009**, *19*, 5220.
[36] M. D. Susman, Y. Feldman, A. Vaskevich, I. Rubinstein, *ACS Nano* **2014**, *8*, 162.
[37] M. S. José, A. Emilio, D. G. Julian, G. Alberto, J. Javier, O. Pablo, S.-P. Daniel, *J. Phys.: Condens. Matter* **2002**, *14*, 2745.
[38] H. Bao, W. Zhang, D. Shang, Q. Hua, Y. Ma, Z. Jiang, J. Yang, W. Huang, *J. Phys. Chem. C* **2010**, *114*, 6676.